Mon. Not. R. Astron. Soc. **000**, 1–10 () Printed 25 October 2018 (MN LATEX style file v1.4)

A TiO study of the dwarf nova IP Pegasi

G. Beekman, M. Somers, T. Naylor and C. Hellier
Department of Physics, Keele University, Staffordshire ST5 5BG

Accepted ???. Received ???; In original form ???.

ABSTRACT

We present red spectra in the region $\sim \lambda$7000–8300Å of the eclipsing dwarf nova IP Peg, with simultaneous narrow-band photometry centered at 7322Å. We show that by placing a second star on the slit we can correct for the telluric absorption bands which have hitherto made the TiO features from the secondary star unusable. We use these TiO features to carry out a radial velocity study of the secondary star, and find this gives an improvement in signal-to-noise of a factor two compared with using the NaI doublet. In contrast with previous results, we find no apparent ellipticity in the radial velocity curve. As a result we revise the semi-amplitude to $K_2 = 331.3 \pm 5.8$ km s^{-1}, and thus the primary and secondary star masses to $1.05^{+0.14}_{-0.07}$M$_\odot$ and $0.33^{+0.14}_{-0.05}$M$_\odot$ respectively. Although this is the lowest mass yet derived for the secondary star, it is still over-massive for its observed spectral type. However, the revised mass and radius bring IP Peg into line with other CVs in the mass-radius-period relationships.

By fitting the phase resolved spectra around the TiO bands to a mean spectrum, we attempt to isolate the lightcurve of the secondary star. The resulting lightcurve has marked deviations from the expected ellipsoidal shape. The largest difference is at phase 0.5, and can be explained as an eclipse of the secondary star by the disc, indicating that the disc is optically thick when viewed at high inclination angles.

Key words: novae, cataclysmic variables – binaries: close – binaries: spectroscopic – binaries: eclipsing – stars:fundamental parameters – stars: individual: IP Peg

1 INTRODUCTION

IP Peg is a dwarf nova which brightens by ∼2 mag every 100 days or so, with each outburst lasting ∼2 weeks, and is important because it is the brightest known eclipsing dwarf nova above the period gap. The eclipses give tight constraints on the geometry of the system, and in combination with other data, such as radial velocity studies, allow the masses of the two stars to be determined. We should thus be able to compare the mass, radius and density of the secondary star with those of main sequence stars, and learn something of its structure and evolution. Unfortunately the radial velocity curve of the secondary star in IP Peg is problematical, being apparently elliptical (Martin et al. 1989, henceforth M89). The star is believed to be in a circular orbit, and the apparent ellipticity is thought to be due to irradiation of the secondary star (although we shall present an alternative explanation in Section 6.4), and an uncertain correction must be applied before the binary parameters can be determined. The result is acutely embarrassing. Smith & Dhillon (1998) collect together all the available masses, radii and spectral types for CVs. IP Peg is one of the few objects that does not rely on the dubious method of using the accretion disc lines to determine the white dwarf radial velocity, and so should give reliable parameters. However, in all the relationships IP Peg is a persistent offender, lying well clear of the supposedly less reliable points in both the mass vs. orbital period and mass vs. spectral type diagrams.

A further complication is presented by the lightcurve of the system. High-speed photometric observations show a light curve dominated by a bright spot and a deep eclipse. The eclipse is that of the bright spot and white dwarf by the secondary star, superposed on a more gradual disc eclipse. Unfortunately the bright spot ingress overlaps with that of the white dwarf, making the ephemeris determination more problematical. Wood & Crawford (1986) were able to use their high-speed photometric observations to derive an ephemeris for IP Peg based on white dwarf egress timings. Later observations by Wood et al. (1989) and Wolf et al. (1993) show that the white dwarf egress varies markedly in strength and duration (10s to 300s).

In this paper we present red spectroscopy and photometry of IP Peg. The observations and their reduction are explained in Section 2. After that the paper divides into two main threads. The first is the radial velocity study and its results. The extraction of the velocities is described in Section 3 after which we discuss the summed spectra and new ephemeris (Sections 4 and 5). In Section 6 we discuss the absence of apparent eccentricity in our data, and con-

clude the system has changed in some way. We use our radial velocity semi-amplitude to derive new system parameters in Section 7. The second thread, isolating the lightcurve of the secondary star, is explored in Section 8.

2 OBSERVATIONS

Photometry and spectroscopy of IP Peg were obtained over four nights in 1995 October from the 2.5-m INT and 1.0-m JKT on La Palma. Only two nights of photometry were taken – simultaneous with the spectroscopy (see Section 2.4). Table 1 contains a log of the observations.

Data from the AAVSO show that in the latter half of 1995 IP Peg underwent two outbursts, one in mid-September and one in mid-December. The data presented in this paper were taken in the first week of October, approximately two weeks after the end of the mid-September outburst, and are thus during quiescence.

2.1 Photometry

Data were taken with the JKT on 1995 October 4th & 5th using an EEV7-chip with a scale of 0.31 arcsec per pixel. A narrow band (FWHM=46Å) OII filter with maximum transmission at a wavelength of λ7322Å was used on both nights.

The images were processed by subtracting off a single bias image in the case of the Oct. 4th data, and a median of three biases for the Oct 5th data. A single sky flat taken at the beginning of each night was used to flatfield the images. The photometry was then extracted using an optimal extraction method (Naylor 1998). The photometry of IP Peg was divided by that of a neighbouring star (the second star placed on the slit during the spectroscopic run—see below) to remove the effects of sky transparency variations and, thus, the photometry is relative. The phase-folded light curves for both nights are shown in Figs. 1 and 2 with the bright-spot hump at $\phi \sim -0.2$ and the primary eclipse at $\phi = 0.0$.

2.2 Spectroscopy

Data were taken on 1995 October 4th, 5th, 9th and 10th with the INT, using a TEK4-chip with a scale of 0.33 arcsec per pixel, but binned by a factor two in the spatial direction. A two-arcsec slit was used set at PA 58.7 degrees to obtain the spectrum of a neighbouring star simultaneously (the star used to divide the IP Peg photometry by—see above). This allowed us to correct for slit losses (see Section 2.4). The R831R grating was used on the 4th and 5th, giving ∼1.22 Å per pixel; the R1200R grating was used on the 9th and 10th, giving ∼0.84 Å per pixel. An arc spectrum was taken each time the telescope's position on the sky was changed (∼ every hour). The nights of the 4th and 5th were generally clear but the nights of the 9th and 10th were affected by cloud, especially so the data of the 9th. An exposure time of 600s was used on the 4th, 5th and 9th: 400s on the 10th.

The images for each night were first bias subtracted. Tungsten flats taken each night were then used, after dividing by fitted low-order polynomials, to flatfield the images. Extraction of the spectra was performed using an optimal extraction method (Horne 1986, Robertson 1986), and then wavelength calibration was done using low-order polynomial fits to the appropriate arc spectra.

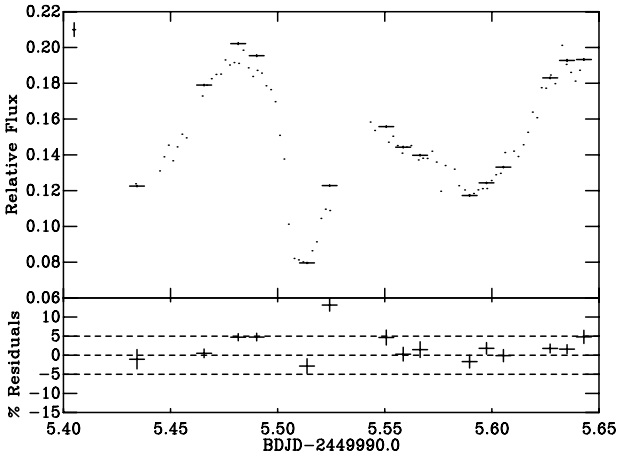

Figure 1. The lightcurves obtained from the photometry (dots) and spectroscopy (bars). The lower panel shows the percentage residuals between the two, calculated as $100.0 * (R_{\rm spec} - R_{\rm phot})/R_{\rm phot}$. The point in the top left of the upper panel represents the average size of a photometric error. Data taken on 1995 October 4th.

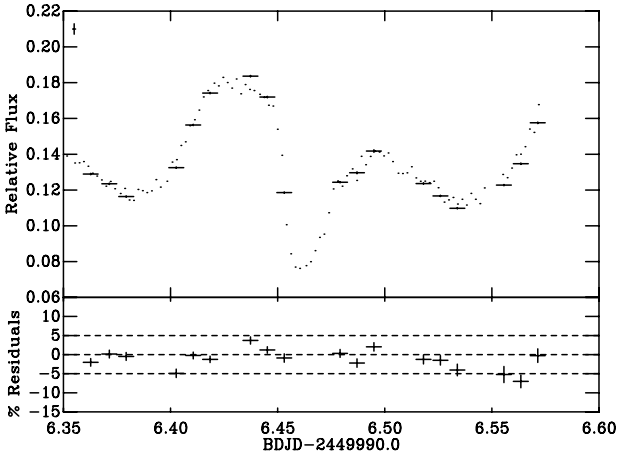

Figure 2. As previous figure but for the data taken on 1995 October 5th.

2.3 Removing the effects of Earth's atmosphere

Normally, one observes a standard star (usually a near-featureless O star) at regular intervals throughout the night to divide the program star by. Here, we use the second star placed on the slit and observed simultaneously with IP Peg. This has the advantage that it avoids the assumption of uniformity of atmospheric absorption with position and time. Fig. 3 shows that the atmospheric absorption has been well corrected, including the large bands near 7600Å.

The disadvantage of this technique is that the star may not be as featureless as one would like, since its main selection criterion is proximity to the target star. Comparing blue spectra of the star with those in Jacoby, Hunter & Christian (1984) shows it to be a late F-star. Such stars are good

Table 1. Journal of observations of IP Pegasi

Date (Oct. '95)	No. of Frames	Wavelength Region (Å)	Exposure Time (sec)	Phase Covered	Mean Seeing (arcsec)
Photometry:					
4th	81	OII filter	120	0.51–1.82	2.17
5th	100	OII filter	120	0.31–1.70	1.65
Spectroscopy:					
4th	18	7100–8300	600	0.38–1.03	1.85
5th	18	7100–8300	600	0.38–1.70	1.42
9th	22	7000–7800	600	0.56–1.72	1.78
10th	39	7000–7800	400	0.83–1.79	1.98

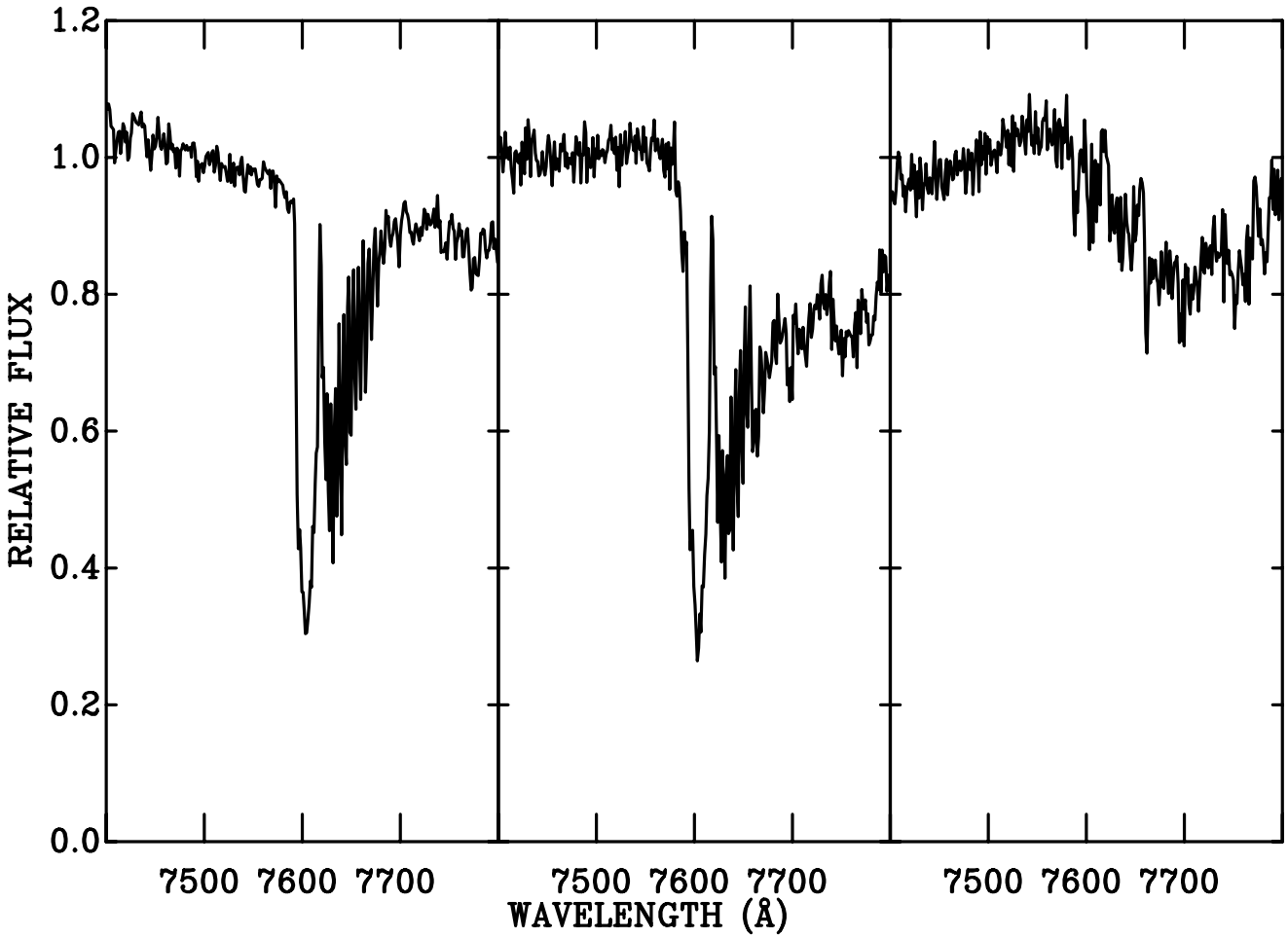

Figure 3. This figure shows the correction for the atmospheric 'A'-band near λ7600Å. The left hand panel is the second star on the slit; the center panel is the uncorrected IP Peg spectrum; the right hand panel after correction. All the spectra have been normalised to one at 7500Å. Note how the drop of the TiO band heads (7550-7650Å) and the KI lines (7650 and 7700Å) become visible after correction.

atmospheric calibrators at low resolution (see Mason et al 1995), but at the intermediate resolutions we used weak absorption features are present. In Fig. 4 we have averaged all our higher-resolution divided spectra with no velocity shift, and can see these features as "emission" lines superimposed on a velocity smeared M-star spectrum (since we have not corrected to the rest frame of the secondary star). The features are weak (normally around a couple of percent, with a few at 10 percent) and as we shall show in Sections 3 and 4, have a negligible effect our radial velocity study and final summed spectrum.

2.4 Relative spectrophotometry

During our spectroscopic run with the INT, two nights of photometric data (simultaneous with the spectroscopic

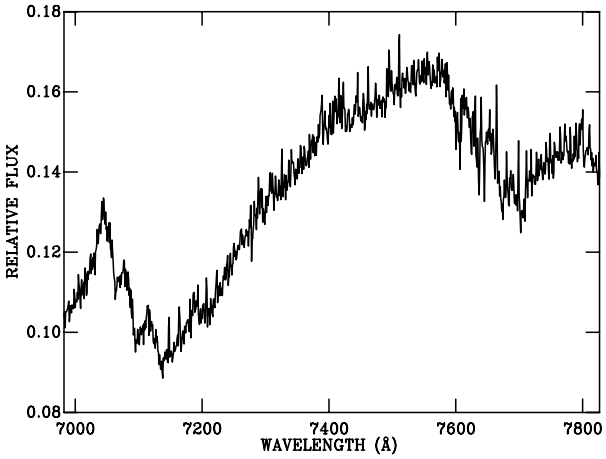

Figure 4. The result of a simple mean of the spectra which result from dividing the IP Peg spectrum by the second star on the slit. Only the higher-resolution spectra (1995 Oct 9 and 10) have been used.

data) were taken with the JKT to test the two-star spectrophotometry technique. The wavelength region of the spectroscopy corresponding to the photometry was isolated and summed according to the weights of the OII filter. After summing, the spectrophotometry of IP Peg was divided by the similarly summed flux from the second star on the slit.

Figs. 1 and 2 show the photometric data over-plotted on the spectroscopic data. The lower panels in the figures show the percentage residuals between the two, calculated as $100.0 * (R_{\rm spec} - R_{\rm phot})/R_{\rm phot}$. Where more than one photometric point is coincident with a spectroscopic one, a simple average of them is taken. For the spectroscopy point covering primary-eclipse egress in the data of 1995 October 4th, the exposure was too large long sample the fast rate of change in brightness properly. This resulted in the relatively large residual seen here. Ignoring this point in the analysis, the average residual size for the nights of the 4th and 5th are 3.28% and 2.80%, respectively. That is, the difference between relative photometry and relative spectrophotometry is only at the few percent level and, for the most part, lies within the error of the photometry. Thus the real difference is probably well within the measurement errors. This shows that performing relative spectroscopy by the inclusion of a second star on the slit works well.

This result is apparently in contradiction with the work of Webb et al. (2000). They performed a similar experiment to ours, obtaining spectroscopic observations of the low-mass X-ray binary J0422+32, again with a second star on the slit. When they compared the relative photometry from their spectroscopic observations with that from simultaneous photometry they found differences of order 15 percent. The author in common between these two papers has no explanation as to why this should be so, though we note that IP Peg is much brighter, and that a broadband filter was used for J0422+32.

3 A RADIAL VELOCITY STUDY

We used an iterative procedure to determine the radial velocity curve of IP Peg, in which a summed spectrum (created after each iteration) is used as the template. This technique is similar to that used by Mukai & Charles (1988) and Horne, Welsh & Wade (1993). First, the mid-white dwarf egress timings of Wood et al. (1989) and Wolf et al. (1993) were fitted with a linear ephemeris, and this ephemeris was initially used to phase all of our spectra. The radial velocity semi-amplitude (K_2) value from M89 was then used to assign a stellar radial velocity component to each spectrum for a given phase ϕ by assuming a circular orbit for the red star of the form $K_2 \sin(2\pi\phi_i)$, where ϕ_i is the phase of spectrum i. Each spectrum was then Doppler-shifted by its orbital radial velocity; all such shifted spectra were then co-added into a grand-sum spectrum. This grand-sum spectrum (less the spectrum of interest — see later) was then used as a template spectrum against which to cross-correlate all the individual spectra to obtain a radial velocity study.

The velocity extraction process is run iteratively. The velocities from the initial set of cross-correlations are fitted with a sine wave to return a new K_2-value and correction to phase zero; each individual spectrum is then assigned a new phase and new radial velocity from this second generation ephemeris and K_2-value; each spectrum is then shifted by these new velocities and combined to make a new orbit-averaged template spectrum; the spectra are then cross-correlated against this new average, new velocities extracted and so on, and the whole process repeats until convergence.

The process was considered to have converged when the correction to phase zero was less than 0.001 of the orbital period, corresponding to a correction of less than 14 seconds. This value was chosen because tests showed that beyond this, no significant improvement within the errors of the fit was achieved. Convergence typically occurred within ten iterations. A small number of spectra returned dubious velocities; these spectra were of lower signal-to-noise (mainly those of 1995 October 9th, due to occasional cloud), and were removed from the analysis.

Note that to avoid any danger of 'self' cross-correlation, the spectrum being correlated is not used in creating the average-spectrum template against which it is being cross-correlated. This results in a new template being created for each individual spectrum, but the large number of spectra which adequately sample the orbit ensures that the template spectrum is, to all intents and purposes, identical throughout.

The first two nights of data were taken at a slightly lower resolution than the last two, so the data were split into high and low resolution data sets and each one treated separately. For both sets of data, two regions were used in the cross-correlation but only one region was used at a time. These regions were a 115Å-wide region from λ7105–7220Å, and a 170Å–wide region from λ7560–7730Å. The slightly different wavelength coverage between the two data sets allowed the shorter wavelength cross-correlation region in the slightly higher resolution data set to be extended blue-wards to λ7000Å.

Table 2 presents the results of this study for the two regions used in each data set. A weighted mean (labelled

Table 2. Radial velocity data using an orbital-average as template

λ	Notes	N	K_2	T_0-2449998.0[2]	σ_c	σ_e	F	p[1]
7105–7220	TiO	31	353.8 ± 14.1	0.51609(86)	32.14	31.67	0.404	0.671
7560–7730	TiO,K	32	325.6 ± 14.3	0.51722(95)	33.92	33.41	0.424	0.658
7000–7220	TiO	59	310.6 ± 9.4	0.51841(73)	32.42	31.78	1.183	0.314
7560–7730	TiO,K	59	344.3 ± 9.5	0.51612(64)	33.01	32.88	0.220	0.803
	$w\Sigma$		331.3 ± 5.8	0.51692(39)				
7670–8319	M89 region	32	327.7 ± 16.1		30.11	30.11	0.00	1.00

[1]Orbit is consistent with being circular for $p \geq 0.05$.
[2]Numbers in brackets are the errors on the same number of figures immediately to their left.

$w\Sigma$ in the table) of these results provides us with a new mid-white dwarf eclipse (*not* egress) timing and K_2. The individual radial velocity curves are shown in Fig. 5 with a circular orbit fit using the above weighted mean values over plotted as a full line; the individual orbital fits of Table 2 are over-plotted as dashed lines. The quoted error is the 68% confidence interval ('1σ') calculated for two free parameters (Lampton, Margon & Bowyer 1976). To derive this error the radial velocity points were given equal weight, and a χ^2_ν assumed for the best fit.

We compared the signal-to-noise we obtained using the TiO bands with that from the more traditional NaI doublet. The gain using the new technique is about a factor two in signal-to-noise if the results from the two TiO bands are averaged. We also tried cross-correlating each spectrum against an M-star template instead of the mean IP Peg spectrum. There was an increase in noise for the fits to these data, presumably because the mean spectrum gives a better match to the spectral type than any template star.

Finally we wished to ascertain whether the weak F-star features introduced by our technique for removing telluric absorption (see Section 2.3) had affected our values for the radial velocity. Specifically, there was a concern that it would introduce a signal at zero velocity shift, which might reduce the semi-amplitude. During the run we took several observations of early-type stars to check our correction technique. We chose a pair of observations where an O-star corrected the observation of the second star on our slit well, yielding a telluric absorption corrected spectrum of this star. We then divided our corrected spectra of IP Peg by this spectrum, thus doubling the strength of the F-star features. We then repeated our cross correlation analysis for Oct. 4 and 5. The derived semi-amplitude changed by less than the error (+7 km s^{-1} for 7105-7220Å and -4 km s^{-1} for 7560-7730Å). It should be noted that this is an over-estimate of how much the F-star affects our study, since we will also have introduced noise, and poor atmospheric correction, all of which might tend to decrease the semi-amplitude. Despite this, it is clear that the second star on the slit makes a negligible contribution to the cross-correlation function, for reasons we explain in the next Section.

4 THE SUMMED SPECTRUM

Fig. 6 shows the final Doppler-shifted weighted-mean spectrum. The reasons for our choice of cross-correlation bands should now be clear. The first corresponds to the TiO band heads around 7100Å, the second to the TiO band heads

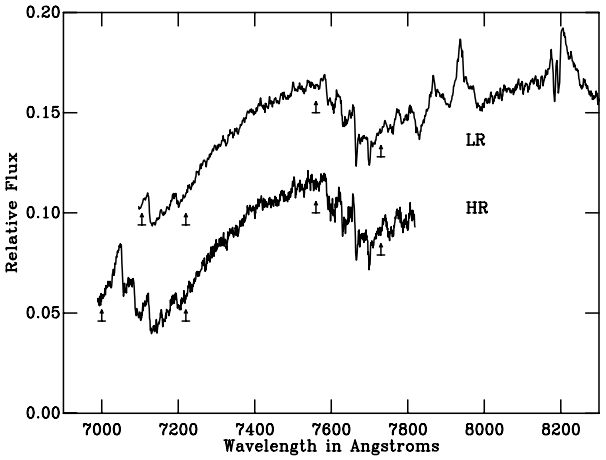

Figure 6. The Doppler-shifted, averaged spectra of IP Peg taken during 1995 October. LR is the lower resolution data taken on the nights of the 4th & 5th (upper spectrum); HR is the higher resolution data taken on the 9th & 10th (lower spectrum). Lower limit symbols mark the boundaries of the cross-correlation regions used in the radial velocity study.

and KI lines (λ7764.9, 7699.0Å) near 7600Å. The final feature obviously from the secondary star is the NaI doublet (λ8183.3, 8194.8Å).

The emission features are harder to identify, so to aid this process we show the sums of spectra in four phase ranges near phase zero in Fig. 7. In this, and Fig. 6 we can see emission features around 7770Å, 7800Å, 7870Å, 7930Å and 8200Å. These features are all broad, and weaken or disappear when the disc is eclipsed in the phase 0.95-0.05 spectrum of Fig. 7. This suggests a disc origin for all these lines. The easiest to identify is the emission around 8200Å, which is where the Paschen series converges, but we can also expect disc emission from the NaI doublet, and perhaps CaII 8203Å and maybe even HeII 8237Å. Friend et al. (1988) identify the OI triplet at $\lambda\lambda$7771.9, 7774.2 and 7775.4Å, which coincides with our 7770Å feature. This leaves three features still unexplained, of which only the 7800Å feature appears in M89.

In principle there is a contribution to this spectrum from the F-star used for telluric correction. However, as stated in Section 2.3 the strongest features are around 10 percent of the continuum level. As the summed spectrum is velocity shifted, these features are smeared out over 600km s^{-1}, or 15 pixels, making them less than 1 percent in depth. The lines will be similarly smeared in the template spectra

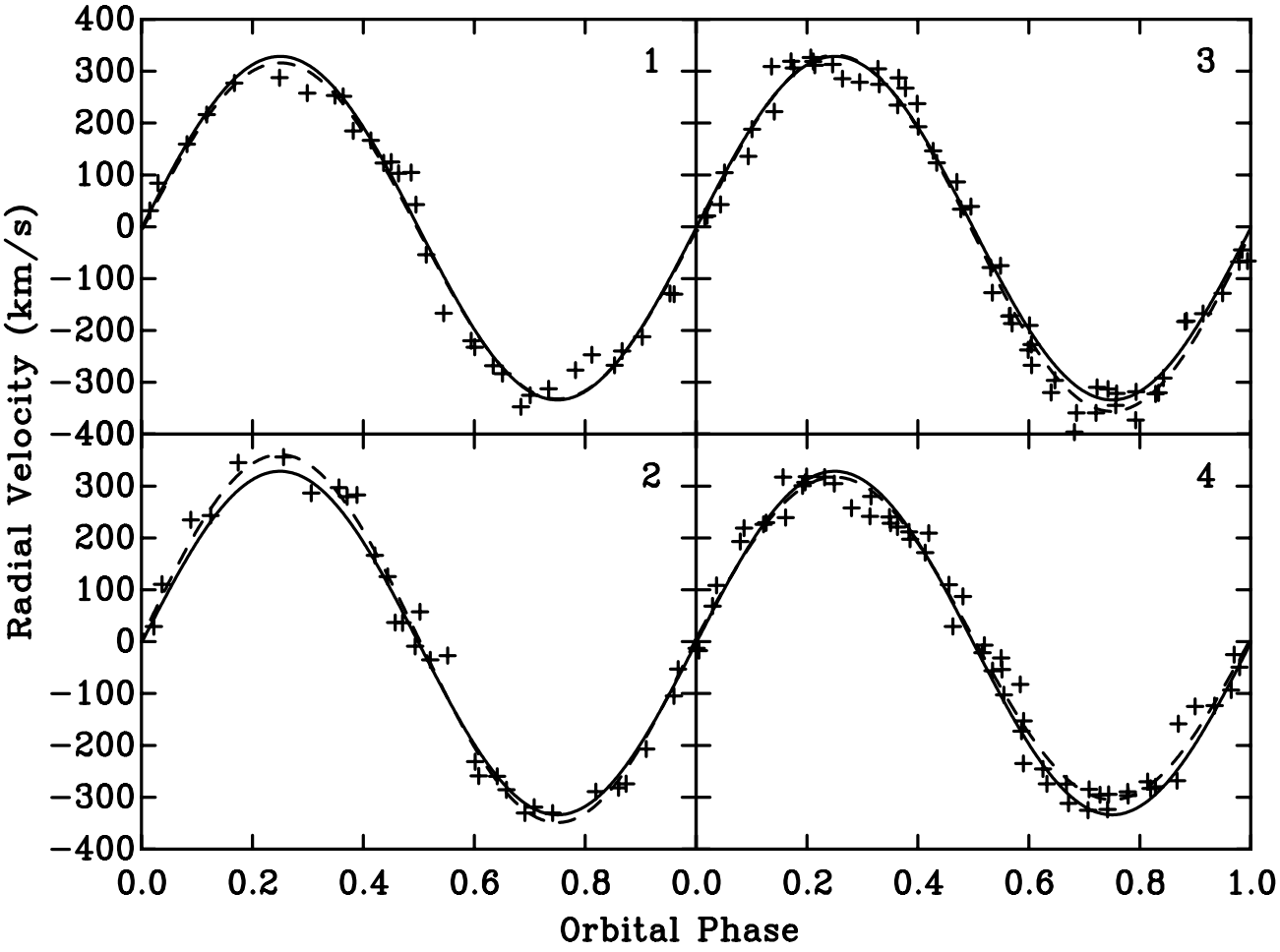

Figure 5. Extracted IP Peg radial velocity curves. (1) The region 7560–7330Å for Oct. 4th & 5th; (2) the region 7105–7220Å for Oct. 4th & 5th; (3) the region 7560–7730Å for Oct. 9th & 10th; (4) the region 7000–7220Å for Oct. 9th & 10th. The dashed lines are the best fit to each panel (see Table 2). The full lines are the weighted mean of the individual fits.

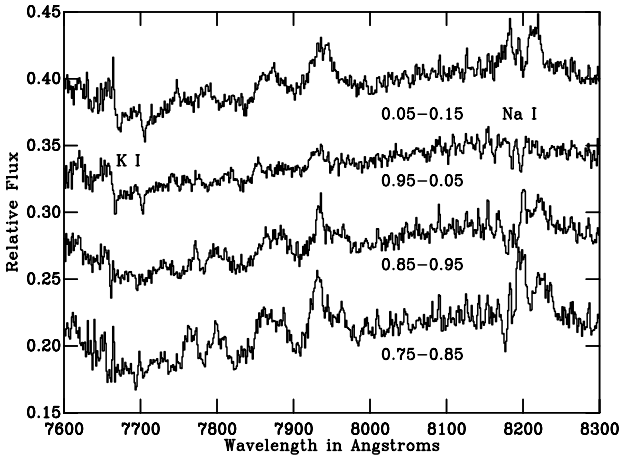

Figure 7. Phase-binned spectra of IP Peg from 1995 October 4th & 5th. Phase ranges are marked, as are the KI and NaI absorption features.

used for the cross-correlation, which is presumably why they have no significant effect on the radial velocity study.

5 A NEW EPHEMERIS

Our spectroscopically derived eclipse timing-point and that of M89, both corrected to time of mid-white dwarf egress, were added to the photometric timings of Wood et al. (1989) and those of Wolf et al. (1993). All timings were converted to TDB. A linear ephemeris was then calculated to give

$$\mathrm{JD(TDB)}\ \ \mathrm{T_{egress}} = 244\ 7965.891\ 44(5) + \mathrm{E} * 0.158\ 206\ 17(3)$$

which is for the time of mid-white dwarf *egress*. Fig. 8 shows the $O-C$ plot for this ephemeris. We note in passing that the $O-C$ residuals calculated from the linear ephemeris can be fitted by a sine wave with parameters close to those given in Wolf et al. (1993), which they interpreted as a third body in the system.

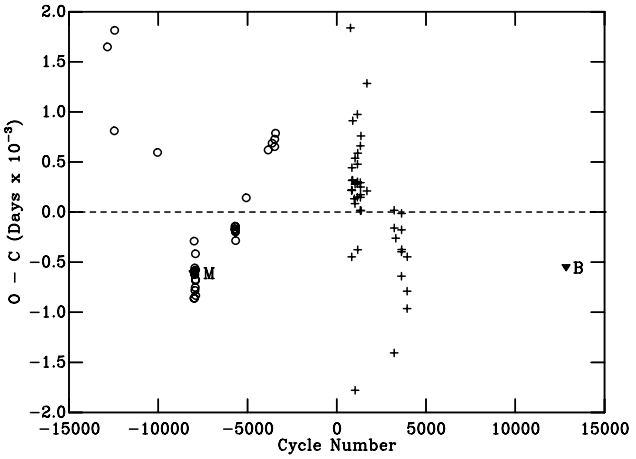

Figure 8. The O-C plot for the mid-white dwarf egress ephemeris from the high-speed photometry timings of Wood et al. 1989 (circles), Wolf et al. 1993 (crosses) and the spectroscopic points from M89 and this paper (filled triangles, also marked with M and B for clarity).

6 THE APPARENT ECCENTRICITY

6.1 Are the new data consistent with a circular orbit?

M89 found that an elliptical orbit was a better fit to their radial velocity data than a circular one. Here, we test our spectra for evidence of eccentricity.

We fitted each red-star radial-velocity data set with a circular orbit of the form

$$V = \gamma + K_2 \sin(2\pi[\phi_i - \phi_0])$$

and then an elliptical orbit of the form (e.g. Smart 1977, Chap. XIV; Petrie 1962)

$$V = \gamma + K_2[\cos(\nu + \omega) + e\cos(\omega)]$$

recording the mean square deviations (S^2) of the data from the fitted model in each case. In the elliptical orbit ν is the true anomaly of the red star, ω is the longitude of periastron of the red star from the centre of gravity of the system, and e is the eccentricity of the red-star orbit. Following Lucy and Sweeney (1971), we use the F-test

$$F = \frac{N_{\rm obs} - f_{\rm ell}}{f_{\rm ell} - f_{\rm crc}} \left(\frac{S^2_{\rm crc}}{S^2_{\rm ell}} - 1 \right) \quad (1)$$

to determine the significance of the elliptical fit over the circular one. $N_{\rm obs}$ is the number of observations, $f_{\rm ell}$ is the number of degrees of freedom in the elliptical fit, $f_{\rm crc}$ those in the circular fit, and $S^2_{\rm crc}, S^2_{\rm ell}$ are the variances of the data from the circular and elliptical fits respectively, i.e. $S^2 = \Sigma(y_{data} - y_{fit})^2$. This test may be derived from the relationship between the F- and χ^2- distributions (e.g. Bevington 1969, Ch. 10). For both the circular and elliptical fits the systemic velocity, γ, was held fixed at zero since our method of radial velocity extraction uses an orbital-average as a template; the orbital period was also held fixed. The number of free parameters in each fit is then $f_{\rm ell} = 4$ (K_2, e, ν and ω) and $f_{\rm crc} = 2$ (K_2 and ϕ_0).

In statistical terms we are testing the hypothesis that the radial velocity curves are consistent with zero eccentricity. Table 2 shows for each radial velocity data set the probability (p) that this hypothesis is correct, and since p never falls below 30 percent, we must accept the hypothesis.

6.2 Are the new data consistent with the previously measured eccentricity?

Although our data are consistent with a circular orbit, it is still possible that, were they noisy enough, they could also be consistent with an eccentricity at the level measured by M89. So we determined the maximum level of eccentricity that could be present in our data.

For this exercise we fitted simultaneously the velocities from both TiO bands, but retained the separate data sets for each resolution. For each data set we constructed an e-χ^2 space by freezing e at set values but allowing all other parameters (except orbital period, always held fixed) to run free. Imposing the condition that χ^2_ν=1 for the e=0 fit, defines the error for each velocity point. From the 90% confidence interval for five free parameters (Lampton, Margon & Bowyer 1976), both data sets yield an upper limit to any eccentricity in our data of around 0.05.

Thus we conclude that our upper limit to the eccentricity is smaller than M89's detection (0.089±0.020).

6.3 Is the difference in eccentricity due to a difference in technique?

There are two important differences between our measurements and those of M89. They used the NaI doublet, whilst we used TiO; and they cross correlated against an M-star template, whilst we used a velocity-shifted mean of the data. So, we performed a cross-correlation study using the M3.5V template GL27B, over the NaI region used by M89. For testing the significance of the eccentricity we used $f_{\rm ell} = 5$ and $f_{\rm crc} = 3$, since γ is an extra free parameter in each case. The results are shown in Table 2, and show that this study also returns zero eccentricity.

The only remaining difference in technique is that M89 used a slightly different formula for the radial velocity, which breaks down for $e > 0.1$. Although this approximation should not create a problem, for completeness we also tested their table 2 data, labelled M89 in our Table 2. Our code finds a similar eccentricity ($e = 0.094$), rejecting a circular orbit at greater than 99.99% confidence.

6.4 Orbital eccentricity; a discussion

The conclusion is thus inescapable, the apparent eccentricity of the orbit has changed between the observations of M89 and our own. IP Peg is not the only system where an apparent eccentricity has been observed in the radial velocity data. AM Her, U Gem, CH UMa and YY Dra all show significant eccentricities (Friend et al. 1990a,b). The explanation that has been put forward to explain these deviations is irradiation of the secondary star, either by the white dwarf, bright spot or a combination of both. Under this assumption, Davey & Smith (1992) were able to map the distribution of the NaI doublet across the surface of the secondary star. As Davey & Smith point out, there is no

satisfactory theoretical explanation for the asymmetric distributions this model predicts, nor is there any apparent correlation with other parameters which would indicate the presence of strong heating. As our spectra show the NaI doublet to be strongly contaminated by emission from the accretion disc, we put forward an alternative hypothesis, that this contamination, even when it is much weaker, affects the radial velocity curves of CVs.

IP Peg is a stunning example of the random nature of deriving an eccentricity from radial velocity data: it has been observed twice, over the same wavelength region, both times in quiescence (although the M89 data may have been on the decline from a small outburst), both use a similar procedure, both return the same value for the radial velocity of the secondary star and yet one shows an eccentricity while the other does not. The raison d'être for M89's correction to the radial velocity was the apparent eccentricity of the orbit. Significant irradiation would introduce an eccentricity (see M89), so the the absence of such effects (see also Section 8), means that we should not make any correction to our semi-amplitude.

7 COMPONENT MASSES

The mass function

$$f(M) = \frac{PK_2^3}{2\pi G}, \tag{2}$$

where the symbols have their usual meaning, links the dynamical motion of the secondary star to the mass of the unseen component. Using the values obtained in Section 3, we find

$$f(M) = 0.596 \pm 0.031 \;\; M_\odot \tag{3}$$

which acts as a lower limit to the mass (M_1) of the white dwarf star in IP Peg. Using this value, we can calculate masses of the individual components if the mass ratio, $q = M_2/M_1$ (where M_1 is the mass of the white dwarf), and inclination, i, are known using

$$M_1 = (1+q)^2 \frac{f(M)}{\sin^3(i)}; \quad M_2 = qM_1. \tag{4}$$

The mass ratio may be determined by combining our K_2 with the rotational broadening measurement of Catalán, Smith & Jones (2000). They find $V_{rot}\sin(i)$ =125±15 km s^{-1} where

$$\frac{V_{rot}\sin(i)}{K_2} = (1+q)f(q) \tag{5}$$

and $f(q)$ is any of the approximations to the fractional Roche-lobe radius R_2/a. Here we use the approximation due to Eggleton (1983), which gives a mass ratio of $q = 0.322 \pm 0.075$. We derive the inclination using the eclipse width of $\Delta\phi = 0.0863$ from Wood & Crawford (1986). To be consistent with this eclipse width, we must raise our lower limit on q to 0.285, since smaller mass ratios will not produce a long enough eclipse, even if $i = 90$ degrees. This sets the upper bound of the inclination to 90 degrees, and thus our measurement of the inclination is $i = 85.9^{+4.1}_{-2.9}$ degrees. Since the error in $V_{rot}\sin(i)$ dominates the errors for q, i, M_1 and M_2, we can simply use the extreme values of i, with their corresponding values of q in equation 4 to obtain our limits on the component masses. These are $M_1 = 1.05^{+0.14}_{-0.07}\mathrm{M}_\odot$ and $M_2 = 0.33^{+0.14}_{-0.05}\mathrm{M}_\odot$.

Martin et al. (1987) find, from the reduction in cross-correlation errors, that the secondary star is probably closer to M4.5V than M3.5V. From the TiO line-depth ratio, Catalán et al (2000) find the spectral type to be M5±0.5V. Using the observationally derived mass-spectral type relation of Kirkpatrick & McCarthy (1994–their equation (11)), which is supported by the theoretical models of Baraffe & Chabrier (1996), our value of $M_2 = 0.35 \pm 0.08\mathrm{M}_\odot$ implies a spectral type of M2.2±0.6V. The error in the calculated spectral type includes both the error in our mass estimate and the error in the relation itself. For a spectral type of M4V, this same relation returns a mass of $0.18\mathrm{M}_\odot$. Although our mass estimate is now consistent with an M-dwarf, the secondary star in IP Peg is still over-massive for its derived spectral type.

We can also calculate the radius for the secondary star, and for consistency do so using equation (3) of Smith & Dhillon (1998). This gives a radius of $R_2 = 0.40 \pm 0.03\mathrm{R}_\odot$. We can then place the star in the mass-radius-period relationships given in that paper. In all cases IP Peg is now consistent not only with the other CVs, but also with the current semi-empirical and theoretical relationships.

Our value for q is low compared with previous determinations, and although the error bars overlap with those of Wood & Crawford (1986) who find $0.35 < q < 0.49$ from measurements of the bright spot, it is probably inconsistent with that of Wolf et al (1993) who measure $q = 0.6$ (no error given) from a similar technique. Both values rely on the center-of-light for the stream following a ballistic trajectory, which may well not be the case once it begins to interact with the Keplerian flow in the disc. Marsh (1988) also find $q = 0.6$, but his value relies on measuring the radial velocity of the primary using the wings of emission lines from the disc. Long & Gilliland (1999) have shown how this technique is inaccurate for U Gem.

8 THE SECONDARY STAR LIGHTCURVE

Measuring the flux in the TiO bands should allow us to extract the flux of the secondary star alone, assuming there is no contribution to the TiO from the other sources of the light in the system. Wade & Horne (1988) constructed such a lightcurve for the short period dwarf nova Z Cha, by measuring the total flux in the TiO band with respect to a fitted continuum (*i.e.* a flux deficit). Here we undertake a similar study, but using a slightly more sophisticated method.

8.1 The method

If the temperature dependence of the equivalent width of the spectral features is small for the range of temperatures over the secondary star, the flux from the star at any given phase is some phase-averaged secondary-star spectrum multiplied by a scaling factor we refer to as k_ϕ. Thus, if we scale and then subtract the phase-averaged spectrum from the spectrum at a given phase, the residual will be smooth across the TiO bands when we have chosen the right k_ϕ. Since both the phase-averaged spectrum, and the spectrum at the phase

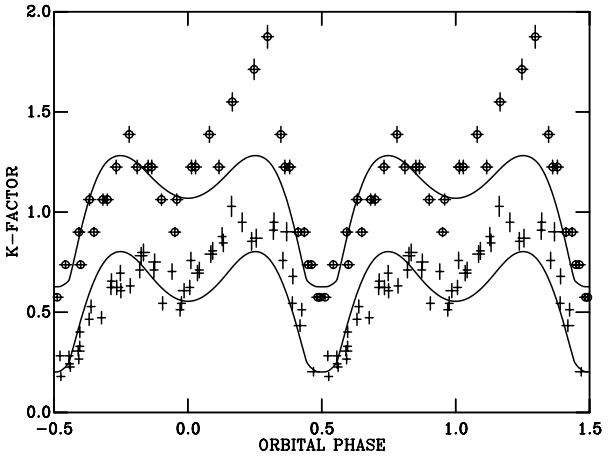

Figure 9. The k_ϕ-factor plotted against phase for the lower resolution data (Oct. 4th & 5th, upper curve, displaced upwards by 0.25 for clarity) and for the higher resolution data (Oct. 9th & 10th, lower curve, displaced downwards by 0.4). The region fitted was 7450–7750Å. Shown over-plotted (full line) is the best-fitting 'ellipsoidal modulation with eclipses' model. The data are plotted twice and k_ϕ is normalised to be about one at phase zero.

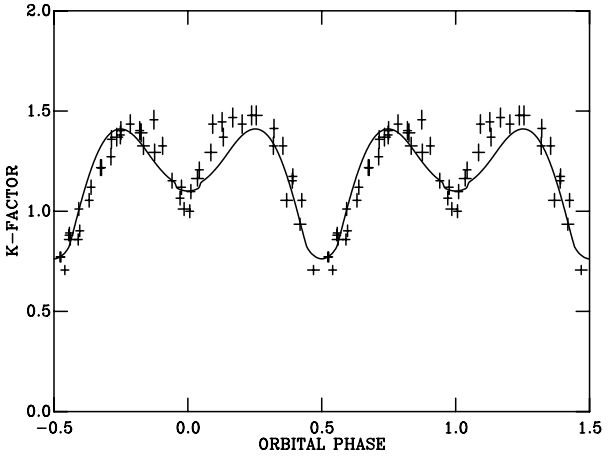

Figure 10. As the previous figure but derived fitting the region 7040–7340Å in the higher resolution data.

under consideration have contributions from the accretion disc, the residual is not simply the accretion disc flux at the phase in question. However, if the disc has a spectrum which is approximately a straight line at all phases, the residual will also be a straight line.

To determine k_ϕ for a given spectrum we subtract from it varying portions of the mean spectrum, fit the residual with a straight line, and evaluate χ^2 for the fit. We then look for the value of k_ϕ which minimises χ^2. To minimise the effect of the assumption of a straight line fit, we evaluate χ^2 over a relatively short fragment of spectrum.

8.2 Results

Fig. 9 shows k_ϕ plotted against orbital phase calculated from the region between 7450–7750Å for both the high and low resolution data sets. The average (χ^2_ν)s (over all spectra) for the individual straight-line fits to the residuals were 2.21±0.23 and 3.59±0.45 for the high and low resolution data, respectively (the error is the standard deviation of the individual fits around these means). Fig. 10 shows k_ϕ plotted against orbital phase for the case of a straight line fit to the region between 7040–7340Å for the low resolution data set.

The most prominent feature in Figs. 9 and 10 is the dip at phase 0.5. The obvious interpretation for this is that it is an eclipse of the secondary star by the accretion disc. This is a rather remarkable result, since the accretion discs of quiescent dwarf novae are normally thought to be optically thin. However, we are viewing the disc in IP Peg at an unusual angle (nearly edge on), and whilst it may be that the discs are optically thin when viewed from the pole, the large column length to the secondary star at phase 0.5 may be enough to obscure it. Alternatively, it may be that there are some optically thick regions in the disc, which cause the eclipse we see.

At other phases the lightcurves are broadly consistent with the double-humped ellipsoidal modulation we might expect. To see just how close they are to this expectation, and prove that the suggestion of an eclipse is at least plausible, we modelled the data using the code described in Ioannou et al (1999). The model is a standard ellipsoidal model with Roche geometry, but importantly for this work, includes the mutual eclipses between the disc and secondary star. Here the disc is assumed to be a cold (i.e. dark) obscurer. We used the parameters derived in Section 7 in addition to a limb darkening coefficient of 0.4, a gravity darkening exponent of 0.08 and a secondary star (pole) temperature of 3375K. We performed a grid search in opening angle and radius to find the best fit to the data.

In Figs. 9 and 10 we plot the best fitting models. This shows that the model can account for the broad outline of the lightcurves, but there are problems in detail. This is reflected by the fact that the best χ^2_ν obtained was 6.1 (for the data of Fig 10), and that all the datasets required a disc radius equal to the Roche-lobe radius of the primary (the maximum we allowed). For the lower resolution data of Fig. 9 the best fit opening angle was 8°, 4° for the higher resolution. For Fig. 10 the opening angle was 3°.

The models throw into sharp relief how the flux at $\phi = 0.75$ is less than that at $\phi = 0.25$. Furthermore, Fig. 9 shows how this asymmetry can vary from night to night. Similar night-to-night variability was seen in the Z Cha TiO flux deficits by Wade & Horne (1988). The asymmetry, and its variability, could be explained by strong irradiation from the bright spot depleting the TiO on the side of the red star facing the bright spot, i.e. the side seen at $\phi = 0.75$. However, this would produce a marked eccentricity in the radial velocity curves deduced from the TiO regions of the spectrum. As shown in Section 6, no significant eccentricity is found from any of the IP Peg absorption features.

The models suggest that the problem is with the data around phase 0.25. This means obscuration of the secondary star by the disc is unlikely, given the star's position well clear of the disc at this phase. Thus we suspect the problem lies with our simple contamination model (a straight line fit). The spectral variations of the disc with time are probably more complex.

9 CONCLUSIONS

The main conclusions from this work are as follows.
(1) There is some form of variability which means that radial velocity studies of the infrared NaI doublet in IP Peg can sometimes return an apparently elliptical orbit. We suspect this is contamination from disc emission.
(2) We strongly recommend the use of TiO rather than NaI for future radial velocity studies. Not only does it avoid the contamination problem described above, but it gives a factor two gain in signal-to-noise.
(3) Our TiO study suggests the radial velocity semi-amplitude for the secondary star should be revised to $K_2 = 331.3 \pm 5.8$km s^{-1}, and as a result the primary and secondary star masses become $M_1 = 1.05^{+0.14}_{-0.07}M_\odot$ and $M_2 = 0.33^{+0.14}_{-0.05}M_\odot$ respectively.
(4) Despite this downwards revision of the secondary star mass, it is still over-massive for its observed spectral type, but now agrees with the current semi-empirical and theoretical mass-radius-period relationships.
(5) The accretion disc eclipses the secondary star in quiescence, implying that, when viewed at high inclination, it is optically thick.

ACKNOWLEDGEMENTS

The INT and JKT is operated on the island of La Palma by the Isaac Newton Group in the Spanish Observatorio del Roque de los Muchachos of the Instituto de Astrofisica de Canarias. Data reduction was carried out on the Keele Starlink node using the ARK software. Data on the outburst state of IP Peg was generously provided by the AAVSO International Database and we gratefully acknowledge with thanks all the variable star observers worldwide who participate in this program. We also thank Sandi Catalán, Janet Wood and Rob Jeffries for useful discussions.

REFERENCES

Baraffe I., Chabrier G., 1996, ApJ, 461, L51
Bevington P.R., 1969, Data Reduction and Error Analysis for the Physical Sciences. McGraw-Hill Book Company, USA.
Catalán M.S., Smith R.C., Jones D.H.P., 2000, MNRAS, submitted
Eggleton P.P., 1983, ApJ, 268, 368
Davey S., Smith R.C., 1992, MNRAS, 257, 476
Friend M.T., Martin J.S., Smith R.C., Jones D.H.P., 1988, MNRAS, 233, 451
Friend M.T., Martin J.S., Smith R.C., Jones D.H.P., 1990a, MNRAS, 246, 637
Friend M.T., Martin J.S., Smith R.C., Jones D.H.P., 1990b, MNRAS, 246, 654
Horne K., 1986, PASP, 98, 609
Horne K., Welsh W.F., Wade R.A., 1993, ApJ, 410, 357
Ioannou Z., Naylor T., Welsh W.F., Catalán M.S., Worraker W.J., James N.D., 1998, MNRAS, accepted
Jacoby G.H., Hunter D.A., Christian C.A., 1984, ApJS, 56, 257
Kirkpatrick J.D., McCarthy D.W., 1994, AJ, 107, 333
Lampton M., Margon B., Bowyer S., 1976, ApJ, 208, 177
Long K.S., Gilliland R.L., 1999, ApJ, 511, 916
Lucy L.B., Sweeney M.A., 1971, AJ, 76, 544
Marsh T.R., 1988, MNRAS, 231, 1117
Martin J.S., Jones D.H.P., Smith R.C., 1987, MNRAS, 224, 1031
Martin J.S., Friend M.T., Smith R.C., Jones D.H.P., 1989, MNRAS, 240, 519 (M89)
Mason K.O. et al, 1995, MNRAS, 274, 1194
Mukai K., Charles P.A., 1988, MNRAS, 226, 209
Naylor T., 1998, MNRAS, 296, 339
Petrie R.M., 1962, in Kuiper G.P., Middlehurst B., eds, Stars and Stellar Systems, Vol. II, Astronomical Techniques, Ch.23. Univ. of Chicago Press, Chicago.
Robertson J.G., 1986, PASP, 98, 1220
Smart W.M., 1977, Textbook on Spherical Astronomy, 6th ed. Cambridge Univ. Press, Cambridge.
Smith D.A., Dhillon V.S., 1998, MNRAS, 301, 767
Wade R.A., Horne K., 1988, ApJ., 324, 411
Warner B., 1995, Cataclysmic Variable Stars. Cambridge Astrophysics Series 28. Cambridge Univ. Press, Cambridge.
Webb N.A., Naylor T., Ioannou Z., Charles P.A., Shahbaz T., 2000, MNRAS, submitted
Wolf S., Mantel K.H., Horne K., Barwig H., Schoembs R., Baernbantner O., 1993, A&A, 273, 160
Wood J., Crawford C.S., 1986, MNRAS, 222, 645
Wood J. et al., 1989, MNRAS, 239, 809